Chapter 17

Evaluation of an Energy Loss-Minimization Algorithm for EVs Based on Induction Motor

Pedro Melo, Ricardo de Castro and Rui Esteves Araújo

Additional information is available at the end of the chapter

http://dx.doi.org/10.5772/52280

1. Introduction

This work addresses the problem of optimal selection of the flux level in induction motors used in electric vehicles (EVs). The basic function of a fully electric powertrain controller is to generate electric torque (force) which is required at any time by the driver. But, it is well-known that the flux level used in a controller for induction motors offers an extra degree of freedom that can be used to maximise energy efficiency. The induction motor is an efficient motor when working close to its rated operating point (Zeraoulia, Benbouzid et al. 2006). However, at light loads the efficiency is greatly reduced when magnetization flux is maintained at nominal value. In induction motor drives for EVs, where real operation conditions are significantly different from rated conditions, the energy saving control is crucial for improving the running distance per charge.

Due to the widespread use of induction motors, its efficiency optimization gave rise to a large number of research publications (Bazzi & Krein 2010). Algorithms for real-time implementation of loss-minimization methods are vital for designing intelligent and optimized EV controllers. Standard methods for induction motor control, including field-oriented control (FOC) or direct torque control (DTC), can be improved in efficiency by using loss minimization control. Basically, there are three different methods to improve the efficiency in induction motors: i) loss model based methods (which is considered in this work), ii) power measure based methods, also known as search controllers; and iii) hybrid controllers that combines the first two methods. The main goal of the present work is to investigate the potential benefits of loss minimization algorithms in EVs powered by induction motors. Accordingly, a detailed simulation case study will be provided which will show that, depending on the type of driving cycle, energy savings up to 12.5% can be achieved. The chapter is organized as follows: Section 2 reviews the basic concepts of rotor field oriented control (FOC). Section 3 introduces the loss minimization method based on a standard mathematical model of the induction motor and gives the value of the flux level

INTECH
open science | open minds

© 2012 Melo et al., licensee InTech. This is an open access chapter distributed under the terms of the Creative Commons Attribution License (http://creativecommons.org/licenses/by/3.0), which permits unrestricted use, distribution, and reproduction in any medium, provided the original work is properly cited.

which maximizes the energy efficiency at given torque subject to voltage and currents limits. In Section 4 the developed EV non-causal simulation model (motor-to-wheel) is presented, while Section 5 includes the simulation results and its analysis for a set of standard driving cycles. Finally, Section 6 contains the main conclusions and some reference to future work.

2. Rotor FOC

In this study, a model based approach was selected for minimizing the induction motor losses (Lim & Nam 2004). This Loss Minimization Algorithm (LMA) was developed in d-q coordinates, considering an equivalent motor model in the synchronous reference frame, as described in section 3. In addition, as we will discuss in a later section, the induction motor controller is also based on rotor FOC. These reasons justify a brief review on induction motor rotor FOC. Figure 1 represents the basic concept of rotor FOC (based on Krishnan, 2001).

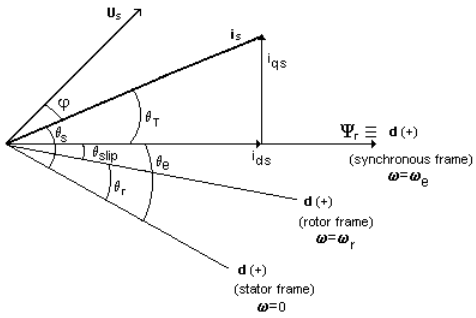

Figure 1. Rotor FOC principle for induction motors

Recall that, in the synchronous frame (ω_e), the rotor magnetic flux (Ψ_{rd}) is aligned with d axis, thus $\Psi_{rd} = \Psi_r$, $\Psi_{rq} = 0$. In the same reference frame, the stator current component i_{ds} is aligned with the rotor magnetic flux, controlling its value. On the other hand, i_{qs} (shifted $\pi/2$ electrical rad from i_{ds}) controls the motor electromagnetic torque:

$$\Psi_r = L_m i_{ds}\left(\text{steady}-\text{state}\right) \tag{1}$$

$$T_t\left(t\right) = K_t \Psi_r i_{qs} \tag{2}$$

From figure 1, it may be seen that i_{ds} and i_{qs} are, respectively, the d and q components of the space vector $\mathbf{i}_s$ in the synchronous reference frame. This way, from the control philosophy perspective, i_{ds} and i_{qs} regulation is implemented in this reference frame; however, from the control hardware perspective, i_{ds} and i_{qs} must be considered in stator reference phase-coordinates (i_a, i_b, i_c). To do that, it is mandatory to obtain i_{ds} and i_{dq} in the static d-q reference, which requires the information about $\theta_s=\theta_e+\theta_T$. The determination of θ_e is the main issue, since $\theta_T = \text{arctg}(i_{qs}/i_{ds})$; θ_e calculation can be accomplished through θ_{slip} and θ_r (see figure 1) – indirect FOC.

Since $$\omega_{\text{slip}} = \omega_{\text{e}} - \omega_{\text{r}} = \frac{L_m}{L_r / R_r}\frac{i_{qs}}{\Psi_r} \quad (3)$$

θ_{slip} is given by:

$$\theta_{\text{slip}}(\text{t}) = \theta_{\text{slip}}(\text{t}_0) + \int_{t_0}^{t} \omega_{slip}\, dt \quad (4)$$

Knowing the instantaneous rotor speed ω_r, one have:

$$\theta_{\text{r}}(\text{t}) = \theta_{\text{r}}(\text{t}_0) + \int_{t_0}^{t} \omega_r dt \quad (5)$$

From figure 1:

$$\theta_{\text{e}}(\text{t}) = \theta_{\text{slip}}(\text{t}) + \theta_{\text{r}}(\text{t}) \quad (6)$$

3. Loss minimization by selecting flux references

The loss-minimization scheme demands the decrease or increase of the flux level depending on the torque. This means that the minimization algorithm selects the flux reference through the minimization of the copper and core losses while ensuring the desired torque requested by the driver. Different techniques for loss minimization in induction motor are presented in the literature (Bazzi & Krein 2010). Recently, (Lim & Nam 2004) proposed a LMA that features a major difference from previous works by taking into consideration the leakage inductance and the practical constrains on voltage and current in the high-speed region, which play a great role in EVs applications. This is an important difference from other works, like (Garcia et al., 1994), (Kioskeridis & Margaris, 1996), (Fernandez-Bernal et al., 2000), where leakage inductance are not considered (although similar motor loss models are included), leading to considerable result differences in the high-speed region. In addition, our work considers the optimization of both positive and negative torque generation with bounded constraints on both current and voltage.

3.1. The LMA method

The implemented method is based on the conventional induction motor model where the iron losses are represented by an equivalent resistance (R_m) modelling the iron losses, placed in parallel with the magnetizing inductance (L_m). A simplification is then considered, allowing a partial decoupling between R_m and L_m: the iron losses are represented by separated circuits with dependent voltage sources (V_{dm}^e and V_{qm}^e). Figure 2 shows the complete equivalent model in the synchronous reference frame.

Considering steady state analysis with low slip values (s) – rotor iron losses may be neglected –, the total motor losses (copper and iron ones) are given by (Lim & Nam 2004):

$$P_{loss} = R_d(\omega_e) i_{ds}^{e\,2} + R_q(\omega_e) i_{qs}^{e\,2} \tag{7}$$

$$R_d(\omega_e) = R_s + \frac{\omega_e^2 L_m^2}{R_m} \tag{8}$$

$$R_q(\omega_e) = R_s + \frac{R_r L_m^2}{L_r^2} + \frac{\omega_e^2 L_m^2 L_{lr}^2}{R_m L_r^2} \tag{9}$$

Where:

i_{ds}^e : d-axis stator current in the synchronous reference frame;

i_{qs}^e : q-axis stator current in the synchronous reference frame;

ω_e : electrical angular frequency;

- R_s; R_r: stator and rotor resistances (respectively);
- R_m: equivalent stator iron losses resistance;
- L_r; L_{lr}: rotor total inductance and rotor leakage inductance (respectively);
- L_m: magnetizing inductance.

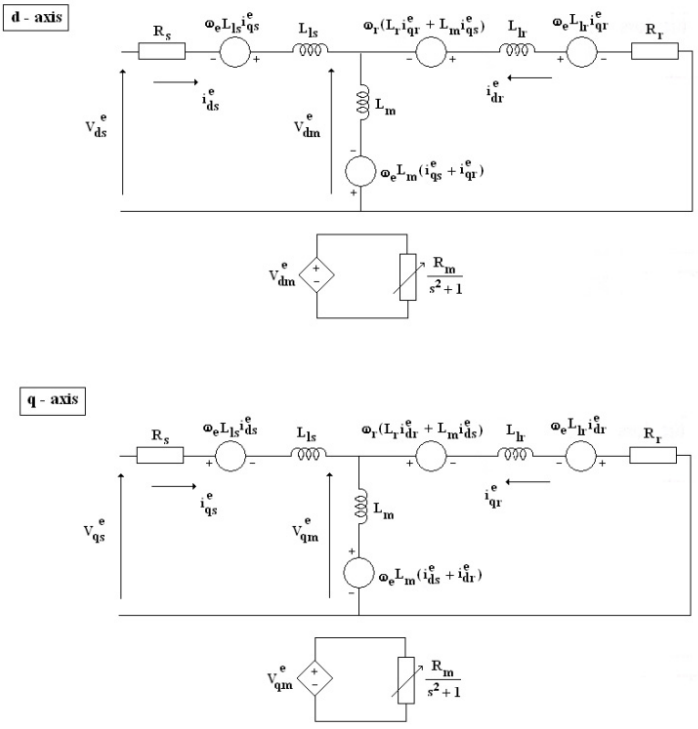

Figure 2. Simplified motor equivalent model (Lim & Nam 2004)

Note that $R_d(\omega_e)$ and $R_q(\omega_e)$ are the direct (d) and quadrature (q) components of the equivalent resistors representing the total losses. Voltage and current constraints (mentioned before) are defined by (neglecting stator resistor drop):

$$(\omega_e L_s i_{ds}^e)^2 + (\omega_e \sigma L_s i_{qs}^e)^2 \le V_{max}^2 \tag{10}$$

$$i_{ds}^{e\,2} + i_{qs}^{e\,2} \le I_{max}^2 \tag{11}$$

Where:

$$\sigma = 1 - L_m^2 / (L_s L_r) \tag{12}$$

σ: induction machine leakage coeficient; L_s: stator total inductance;

V_{max}; I_{max}: motor (or inverter) voltage and current limits, respectively;

An important observation is that voltage constraint depends on the considered ω_e.

The LMA´s goal is to achieve the optimal flux level that minimizes the motor total losses under voltage and current constraints. The motor rated flux level must also be taken into consideration, in order to avoid magnetic saturation. Moreover, the torque developed by the motor cannot be compromised by the LMA implementation. From the mathematical point of view, the LMA algorithm consists in:

$$\min P_{loss}(i_{ds}^e, i_{qs}^e)$$

$$\text{s.t.: (10), (11)}$$

$$i_{ds}^e \le I_{dn} \tag{13}$$

$$T_e = K_t i_{ds}^e i_{qs}^e$$

Where:

I_{dn} : rated d-axis stator current

T_e : electromagnetic torque (steady-state), considering rotor FOC;

$$K_t = \frac{3}{2} p \frac{L_m^2}{L_r} \tag{14}$$

[p: pairs of magnetic poles]

3.1.1. Unconstrained optimization

In the (i_{ds}^e, i_{qs}^e) domain, the optimal flux solution for the region inside the inequality restrictions is achieved through Lagrange multipliers method, since only one restriction is active – the torque one

For one restriction only, the general problem is formulated as follows:

$$\nabla L(i_{ds}^{\ e}, i_{qs}^{\ e}, \lambda) = 0 \tag{15}$$

with: $$L(i_{ds}^{\ e}, i_{qs}^{\ e}, \lambda) = P_{loss}(i_{ds}^{\ e}, i_{qs}^{\ e}) + \lambda (T_e - K_t i_{ds}^{\ e} i_{qs}^{\ e}) \tag{16}$$

where $L(i_{ds}^e, i_{qs}^e, \lambda)$ is the lagrangian associated to the problem, λ is the Lagrange multiplier, $P_{loss}(i_{ds}^e, i_{qs}^e)$ is the cost function and $T_e - K_t i_{ds}^e i_{qs}^e$ is the restriction. Applying first-order optimal condition (15) gives the following equation system:

$$\frac{\partial L}{\partial i_{sq}^{\ e}} = 0 \qquad \frac{\partial L}{\partial i_{sq}^{\ e}} = 0 \qquad \frac{\partial L}{\partial \lambda} = 0 \tag{17}$$

yielding

$$i_{ds}^e = \left(\frac{T_e^2}{K_t^2} \frac{R_q(\omega_e)}{R_d(\omega_e)} \right)^{1/4} \; ; \; i_{qs}^e = \left(\frac{T_e^2}{K_t^2} \frac{R_d(\omega_e)}{R_q(\omega_e)} \right)^{1/4} \tag{18}$$

3.1.2. Constrained optimization

Previously, all the inequalities were considered inactive. In order to obtain the optimal solutions in each restriction boundary, the Lagrange multipliers method is applied for each inequality constraint activation (i.e. only "=" operator is valid), together with the torque one. This way, three non linear algebraic equation systems are defined for the inequality constraints. The optimal i_{ds}^e is given by these systems solutions, since it refers to regions on the border lines of the inequality restrictions.

Table 1 presents the solutions, in (i_{ds}^e, i_{qs}^e) plane, for interior points (zone 0) and for inequality restriction borders (zones 1, 2 and 3).

The voltage and current limits (V_{max}, I_{max} and I_{dn}) lead naturally to three regions of operation referred to as constant torque (low-speed), constant power (midrange speed) and constant power-speed (high-speed), as defined in (Novotny & Lipo, 1996). The transition between constant torque region and power region is characterized by the rated speed (ω_n), which is defined by the interception of inequality restrictions border lines:

$$(\omega_n L_s i_{ds}^e)^2 + (\omega_n \sigma L_s i_{qs}^e)^2 = V_{max}^2 \tag{19}$$

$$i_{ds}^{e\ 2} + i_{qs}^{e\ 2} = I_{max}^2 \tag{20}$$

$$i_{ds}^{e} = I_{dn} \tag{21}$$

Zone	Name	Active Constraints	Solution
0	LMA Operation in Interior Points	$T_e = K_t i_{ds}^e i_{qs}^e$	(18)
1	Max Torque Limit	$T_e = K_t i_{ds}^e i_{qs}^e$ $i_{ds}^e = I_{dn}$	$i_{ds}^e = I_{dn}$; $i_{qs}^e = \frac{T_e}{K_t I_{dn}}$
2	Max. Current Limit	$T_e = K_t i_{ds}^e i_{qs}^e$ $i_{ds}^{e\,2} + i_{qs}^{e\,2} = I_{max}^{\;2}$	$i_{ds}^e = \left(\frac{I_{max}^2 - (I_{max}^4 - 4T_e^2 / K_t^2)^{1/2}}{2} \right)^{1/2}$ $i_{qs}^e = \left(\frac{I_{max}^2 + (I_{max}^4 - 4T_e^2 / K_t^2)^{1/2}}{2} \right)^{1/2}$
3	Max. Voltage Limit	$T_e = K_t i_{ds}^e i_{qs}^e$ $(\omega_e L_s i_{ds}^e)^2$ $+(\omega_e \sigma L_s i_{qs}^e)^2 = V_{max}^2$	$i_{ds}^e = \left(\frac{V_{max}^2 + (V_{max}^4 - 4\omega_e^4 \sigma^2 L_s^4 T_e^2 / K_t^2)^{1/2}}{2(\omega_e L_s)^2} \right)^{1/2}$ $i_{qs}^e = \left(\frac{V_{max}^2 - (V_{max}^4 - 4\omega_e^4 \sigma^2 L_s^4 T_e^2 / K_t^2)^{1/2}}{2(\omega_e L_s)^2} \right)^{1/2}$

Table 1. LMA optimized solutions

The calculated result is:

$$\omega_n = \frac{V_{max}}{L_s} \frac{1}{[I_{dn}^2 + \sigma^2 (I_{max}^2 - I_{dn}^2)]^{1/2}} \tag{22}$$

ω_c is the boundary speed between constant power and power-speed (P_{mec}*ω_e=constant) regions:

$$\omega_c = \frac{V_{max}}{I_{max} L_s} \left(\frac{\sigma^2 + 1}{2\sigma^2} \right)^{1/2} \tag{23}$$

For region 1, the maximum torque is limited by I_{dn} and I_{max}:

$$T_{m1} = K_t I_{dn} (I_{max}^2 - I_{dn}^2)^{1/2} \tag{24}$$

The maximum torque in region 2 is limited by V_{max} and I_{max}:

$$T_{m2} = K_t \frac{[(V_{max} / (\omega_e L_s))^2 - I_{max}^2 \sigma^2]^{1/2} [I_{max}^2 - (V_{max} / (\omega_e L_s))^2]^{1/2}}{1 - \sigma^2} \tag{25}$$

In region 3, the maximum torque is limited by V_{max}, but the current is smaller than I_{max}. So, the current limit does not interfere with T_{m3}:

$$T_{m3} = K_t \left(\frac{V_{max}}{\omega_e L_s} \right)^2 \frac{1}{2\sigma} \tag{26}$$

3.1.3. Optimal I_{ds} generation

For the zone in the (i_{ds}^e, i_{qs}^e) plane limited by restrictions (10), (11) and $i_{ds}^e \leq I_{dn}$, optimal result (18) is valid, meaning that:

$$i_{ds}^e = \left(\frac{R_q(\omega_e)}{R_d(\omega_e)} \right)^{1/2} i_{qs}^e \tag{27}$$

In the border lines of those restrictions, the previous relation can not be considered. So, for region 1, (18) is applied if:

$$i_{qs}^e \leq \left(\frac{R_d(\omega_e)}{R_q(\omega_e)} \right)^{1/2} * I_{dn} \tag{28}$$

The i_{qs}^e upper limit in (28) defines T_{p1}(see Figure 3):

$$T_{p1} = K_t \left(\frac{Rd(\omega_e)}{Rq(\omega_e)} \right)^{1/2} I_{dn}^{\ 2} \tag{29}$$

$$\text{Of course, for:} \quad \left(\frac{Rd(\omega_e)}{Rq(\omega_e)} \right)^{1/2} * I_{dn} < i_{qs}^e \leq (I_{max}^2 - I_{dn}^2)^{1/2} \rightarrow i_{ds}^e = I_{dn} \tag{30}$$

For region 2, (18) can be considered, until the voltage limit (V_{max}) is achieved:

$$i_{qs}^e \leq \frac{V_{max} / (\omega_e L_s \sigma)}{[\sigma^{-2} + R_d(\omega_e) / R_q(\omega_e)]^{1/2}} \left(\frac{Rd(\omega_e)}{Rq(\omega_e)} \right)^{1/2} \tag{31}$$

This way, T_{p2} is given by the following expression:

$$T_{p2} = K_t \frac{V_{max}^2 [R_d(\omega_e) * R_d(\omega_e)]^{1/2}}{[\sigma^2 R_d(\omega_e) + R_q(\omega_e)](\omega_e L_s)^2} \tag{32}$$

Above this limit, i_{ds}^e (and i_{qs}^e) is given by zone 3 solution (table 1).

As stated before, only the voltage limit must be considered for region 3, which means that $T_{p3}= T_{p2}$. Of course, for this region one must consider $\omega_e > \omega_c$.

Figure 3 presents the paths for I_{ds}^* generation in i_{ds}; i_{qs} coordinates (origin-T_p-T_m), considering the three described operation regions. Quadrants I and II are represented, in order to consider both motor and braking modes (optimal i_{ds} paths for quadrant II are symmetric to quadrant I paths).

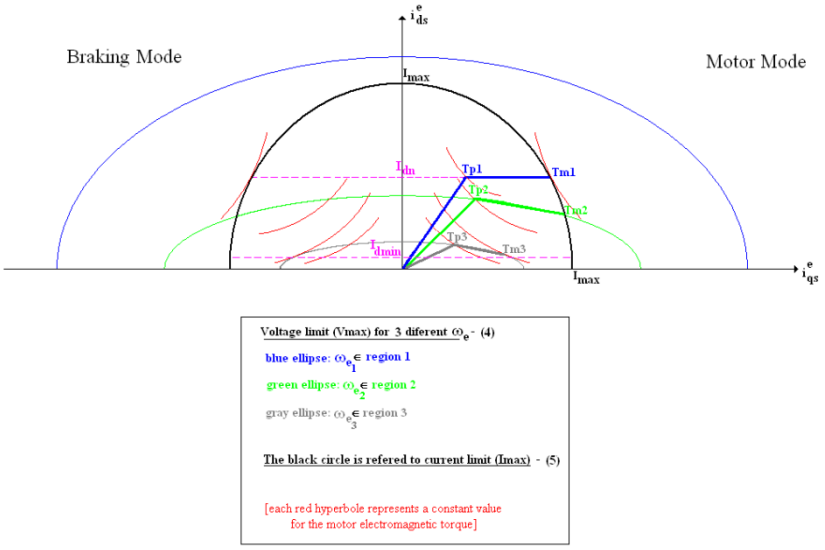

Figure 3. I_{ds}^* paths for ω_{e1} (blue), ω_{e2} (green) and ω_{e3} (gray)

It is clear the linear evolution in the three regions (given by (27)), while in region 3, only voltage limit must be considered, since I_{max} is not reached. After that, in region 1, I_{dn} imposes the optimal path. In region 2 both current and voltage limits (i.e. I_{max} and V_{max}) restrict I_{ds} optimal path, while in region 3, I_{max} most probably is not reached.

3.2. Optimal I_{ds} generation for the simulated induction motor

In order to get some insight on LMA main features, a first set of results is presented in figures 4-6, based on an induction motor, with the following parameters:

[Rs; Rr] (Ω) [0,399; 0,3538]
[Ls; Lr] (H) [59,3; 60,4]*10^{-3}
[ls; lr] (H) [2,7; 3,8]*10^{-3}
Lm (H) 56,6*10^{-3}
Rm (Ω) 350
J(kg m^2) 0,089

Table 2. Induction Motor Parameters (9 kW; 60 Hz; 4 poles; 1750 rpm)

Figure 4 represents the optimal I_d generation for conventional approach, i.e. constant flux +field weakening (CF+FW), and the LMA approach.

Inspecting these results one can find that the LMA influence on I_d* is mostly visible for low torques (T<20 N.m). It is interesting to note that in the high speed zone (>2000 rpm), LMA and conventional flux regulation tend to present closer I_d* values, as the speed increases. Also, for high torque values (above 30 N.m) both approaches have similar performances.

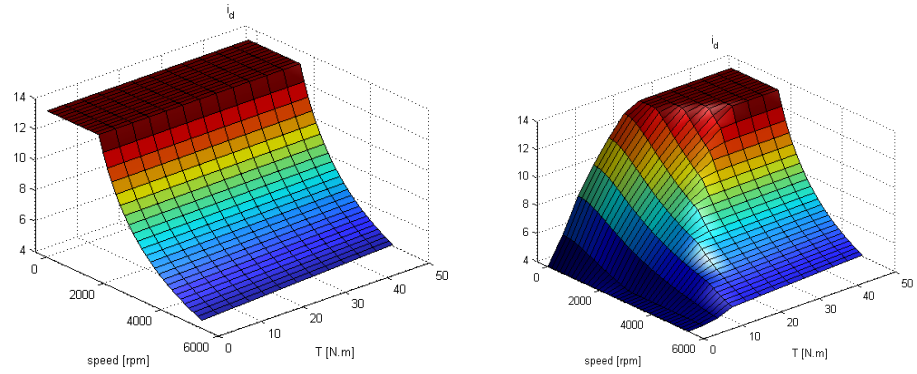

(a) (b)

Figure 4. I_{ds}* generations: a) CF+FW; b) LMA

From the above analysis, it is expectable that the differences in the generation of I_d* lead to different efficiencies curves of the induction motor, which is, indeed, observed in the maps illustrated in Figure 5.

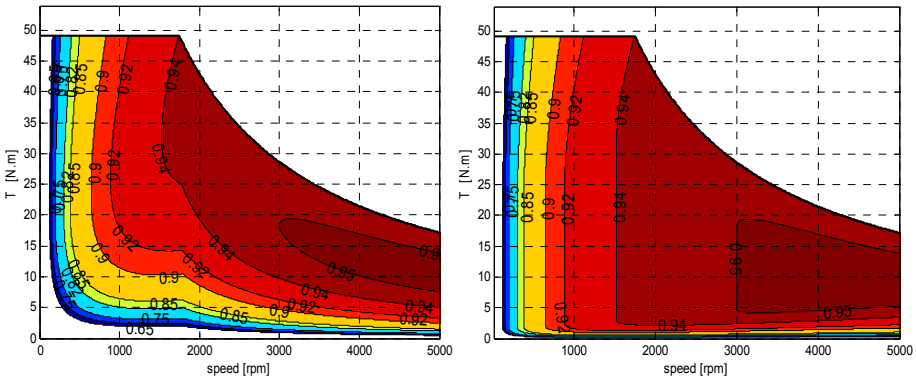

(a) (b)

Figure 5. Induction motor efficiency maps: a) CF+FW; b) LMA

A complementary perspective is presented in figure 6. It can be seen that the main LMA influence region is below 15 N.m (about 30% of motor nominal torque), with a slight behavior difference, according to n<2000 rpm or n>2000rpm: in the former case (coincident with the

constant torque zone), the LMA's efficiency gain is almost constant, while in the late case the energy savings decrease in a smooth way to zero.

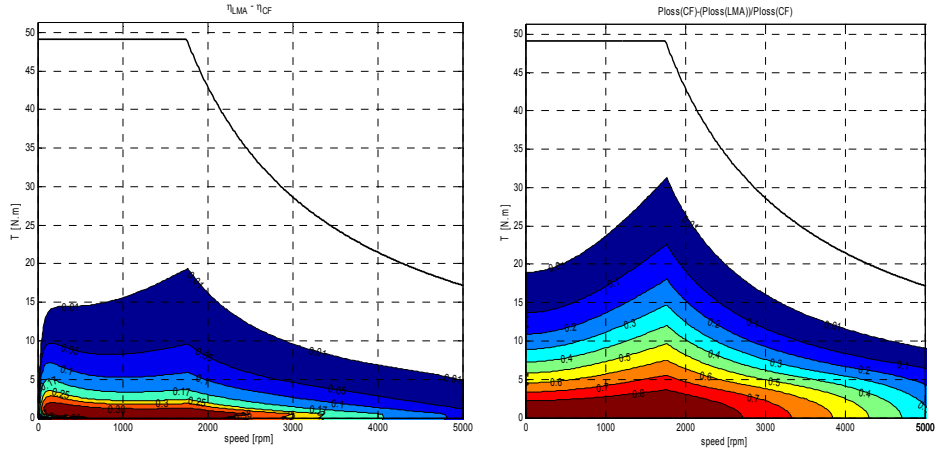

Figure 6. LMA Efficiency gain (a) and relative loss differences (b) compared to (CF+FW)

Naturally, LMA acts directly on motor iron losses, since it regulates I_{ds}. However, it has also an impact in motor copper losses, because it provides a better equilibrium between I_{ds} and I_{qs}, particularly in regions where I_{ds} regulation has wide limits. This can be seen in (7).

As a side-note, when considering the plane surfaces in figure 4 (for $I_{d\ max}$ and $I_{d\ min}$), interesting correlations can be made with figure 3, through ($I_{d\ max}$, $I_{d\ min}$) dashed lines and the torque hyperbolas (e.g. higher torques are provided by $I_{d\ min}$ as the speed grows).

4. Simulation model

To evaluate the LMA´s contributions to the EV energy consumption reduction, and comparing it to the conventional flux regulation, a simulation study was performed with four diferent driving cycles: ECE-R15, Europe: City, 11-Mode (Japan) and FTP-75. Simulation with other drive-cycles was also implemented, but results achieved with these four give a wide overview of LMA´s features. For that purpose, a Matlab/Simulink model was built, which is represented in figure 7.

Basically, I_d* is generated through (CF+FW) method or by the LMA – blocks (3a) and (3b), respectively. The induction motor is controlled by conventional rotor FOC (block 4); the motor model in block 5 is presented in section 4.4. The motor load and speed references are generated based on a particular drive cycle features (block 1), which includes the vehicle dynamic and mechanical transmission models. Finally, block 2 implements the speed controller (based on a proportional+integral(PI) control law) which generates the motor torque reference. In the following sections, the main model blocks are discribed.

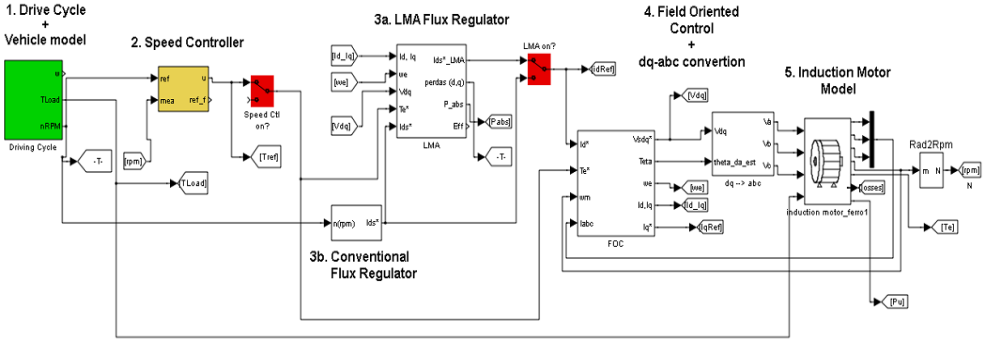

Figure 7. Global simulation model

4.1. Drive cycle+vehicle model

The drive cycles plus the vehicle and mechanical transmission models were implemented with the QuasiStatic Simulation Toolbox (QSS TB), based on Matlab/Simulink, developed by (Guzzella, Amstutz, 2005). The QSS TB library integrates a set of several elements, such as driving cycles, vehicle dynamics, internal combustion engine, electrical motor and mechanical transmisson. Batteries, supercapacitor and fuel cell are also included.

Essentially, it considers a backward (wheel-to-engine) quasi-satic causal model which, based on driving cycle speeds (at discrete times), calculates accelerations and determines the necessary forces, based on the vehicle features and an eventual mechanical transmission. The implemented model includes the QSS TB elements depicted in figure 8.

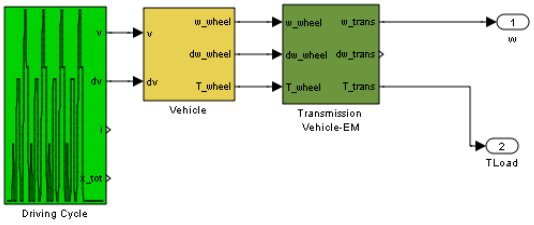

Figure 8. Drive cycle and vehicle/transmission models

The load power demanded to the induction motor ($T_{load}*\omega_r$) considers the drive cycle, vehicle dynamics (rolling and aerodynamic resistance, only in the plane) and also a mechanical transmission with a fixed gear ratio. The vehicle dynamics is modelled by the following equation:

$$M_t \frac{dv(t)}{dt} = F_d(t) - M_t g C_r - \frac{1}{2}\rho C_w A v(t)^2 \qquad (33)$$

Where:
M_t - vehicle mass + equivalent mass of rotating parts;
v(t) – vehicle instantaneous longitudinal speed;
$F_d(t)$ – instantaneous driving force;
g – gravity acceleration;
Cr, Cw – rolling friction coefficient, aerodynamic drag coefficient;
ρ, A – air density; vehicle´s cross section.

Besides the inertia force, associated to vehicle displacement, the inertia of rotating parts (i.e., kinetic energy stored on it caused by rotational movement) should also be considered, since it is the motor(s) who supply it. This is considered in the "equivalent mass of rotating parts" M_t term (see Table 3). It should be noted that driving cycle block output speed (v) and acceleration (dv) are discrete values. The time step size default value is 1 s; however, in order to increase simulation accuracy, its value was fixed in 0,01 s.

Vehicle and transmission parameters are shown in Tables 3 and 4:

Total vehicle's mass (kg)	350
Rotating mass (%)	5
Vehicle´s cross section (m^2)	1,5
Wheel diameter (m)	0,3
Aerodynamic drag coefficient	0,3
Rolling friction coefficient	0,008

Table 3. Vehicle Parameters

Gear ratio	5
Efficiency (%)	98
Idling losses by friction (W)	10
Minimum wheel speed beyond which losses are generated (rad/s)	1

Table 4. Mechanical Transmission Parameters

4.2. Rotor flux setpoint generation

a. LMA

Figure 9 presents the developed LMA block set. R_d and R_q are inputs for the block regions "$w_e<w_n$" and "$w_e>w_n$". Basically, these two elements generate I_{ds}*, according to 3.1.3. As it was described, for zones in the (i_{ds}; i_{qs}) plane limited by restrictions (10), (11) and $i_{ds} \leq I_{dn}$, equation (27) is applied. For the border lines, the three defined regions must be considered: in region 1, I_{ds}* is restricted to its maximum allowable value (I_{dn}); for regions 2 and 3, only voltage limit is considered in I_{ds}* generation restriction. Since $T_{p2}= T_{p3}$, the same block can be used for generating I_{ds}* in these two regions.

Since the flux level should not decrease below a minimum value (I_{d_min}), in order to guarantee that $I_{d\_min} \leq I_{ds} \leq I_{dn}$, two saturation blocks are placed at "$w_e<w_n$" and "$w_e>w_n$" outputs.

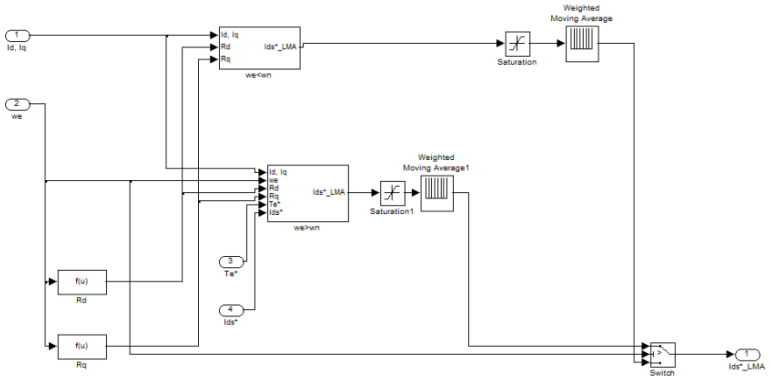

Figure 9. LMA block contents

Figure 10 shows the interior of "w_e<w_n" block.

As it can be seen, I_{ds}* is generated by (27), while I_{ds}<I_{dn}; after that I_{ds}*=I_{dn}. It should be noted that the absolute value of I_{qs} must be used, in order to consider both motor and braking modes.

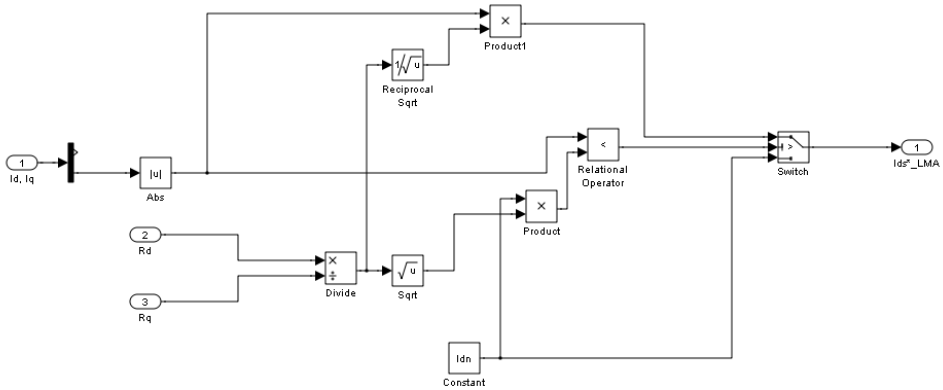

Figure 10. I_{ds}* generation in region 1 (blue path in figure 3)

The block "w_e>w_n" is represented in figure 11. Equation (27) regulates I_{ds}* generation until (31) is no longer true (notice that the absolute value of i_{qs} is compared to the product of "V_{max} restriction" by $(R_d/R_q)^{1/2}$). After that, I_{ds}* is given by zone 3 solution in table 1 (s_3)– "Id* for Vmax restriction border" block. It also should be pointed that when a load point overcomes the voltage limit, the result given by (s_3) is a complex value. In order to deal with this issue, for these situations I_{ds} is taken from the conventional flux regulator.

In contrast with the LMA, the conventional flux regulation (depicted as block (3b) in Figure 7) generates a I_{ds} setpoint according to the following strategy:

$$\begin{cases} I_{ds} = I_{dn} & n \le n_n \\ I_{ds} = n_n/n \cdot I_{dn} & n > n_n \end{cases} \tag{34}$$

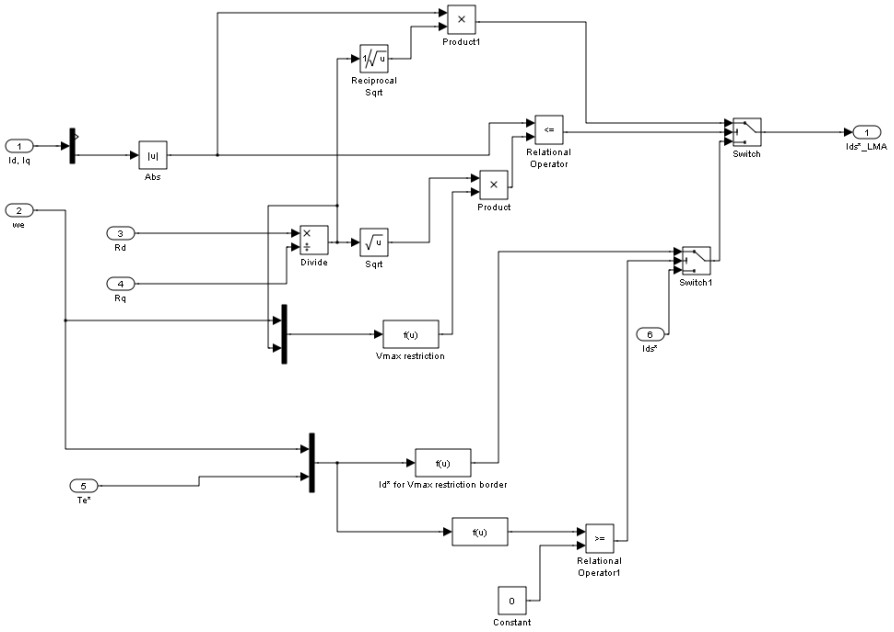

Figure 11. I_{ds}* generation for regions 2 and 3 (green and gray paths in figure 3)

4.3. Rotor indirect FOC

Figure 12 shows the block structure for indirect FOC.

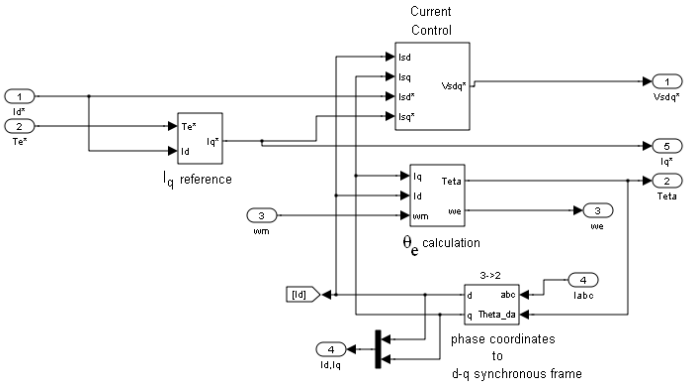

Figure 12. Rotor indirect FOC implementation

Equations (1) and (2) are the basis of "Iq reference" block. Equations (3)-(6) are implemented in "θ_e calculation" block (notice that $\omega_e=\omega_{slip} + \omega_r$). The bottom block considers the coordinates change of instantaneous stator currents, from phase domain to d-q synchronous frame. To do so, the following well known coordinate transformation matrix is applied:

$$\begin{bmatrix} i_{qs} \\ i_{ds} \end{bmatrix} = \frac{2}{3}\begin{bmatrix} \sin\theta_e & \sin(\theta_e - \frac{2}{3}\pi) & \sin(\theta_e + \frac{2}{3}\pi) \\ \cos\theta_e & \cos(\theta_e - \frac{2}{3}\pi) & \cos(\theta_e + \frac{2}{3}\pi) \end{bmatrix}\begin{bmatrix} i_{sa} \\ i_{sb} \\ i_{sc} \end{bmatrix} \quad (35)$$

The "Current Control" block generates stator reference voltage (V_{sdq}*) in synchronous frame (through PI´s current i_{ds} and i_{qs} controllers), which is applied to the motor model, in phase coordinates, in order to make the real instantaneous stator currents to achieve the reference values.

4.4. Induction motor model

Figure 13 presents the induction motor model considered in simulations, which also includes motor iron losses.

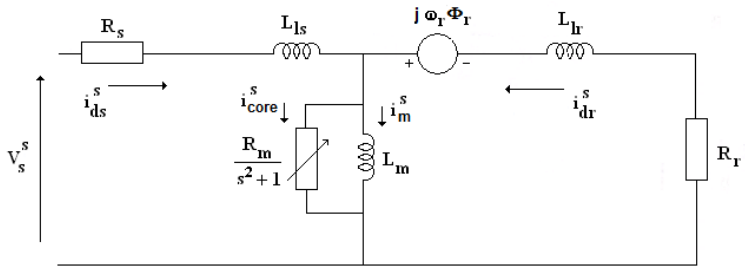

Figure 13. Induction motor model simulated (space vectors in stator reference frame)

When comparing this model to the one considered in LMA (figure 2), the major differences are in parallel (magnetizing) branch. Since core losses currents are not considered in the major circuit, it is expectable that the voltages (V^e_{dm} and V^e_{qm}) on the independent sources are larger compared to the parallel branch voltages in the equivalent model of figure 13. Since core losses are given by $((V^e_{dm})^2+(V^e_{qm})^2)/R_m$, it seems plausible to admit that the core losses in LMA model are higher than the ones in figure 13 model.

Figure 14 shows the simulink implementation of the considered induction motor model (block 5 in figure 7).

5. Simulation results and analysis

An important note is that simulation results were extracted through block 5 (see figure 7), where P_u is obtained directly through T_e*ω_r, based on the drive cycle reference values. In block 3a, Pu is achieved considering P_{ab}-p_{losses} (note that P_{ab}=$u_{sa}i_{sa}$+$u_{sb}i_{sb}$+$u_{sc}i_{sc}$, i.e. the sum of instantaneous power of motor phases a, b, c – see figure 14). Motor losses considered by LMA are based on equation (7). There are some differences in P_u values when block 5 or block 3a are considered, which seems to put in evidence the issue mentioned in 4.4.

For each drive cycle, results are presented following the same pattern: the first figure includes the main results for conventional flux regulation and LMA. The second figure

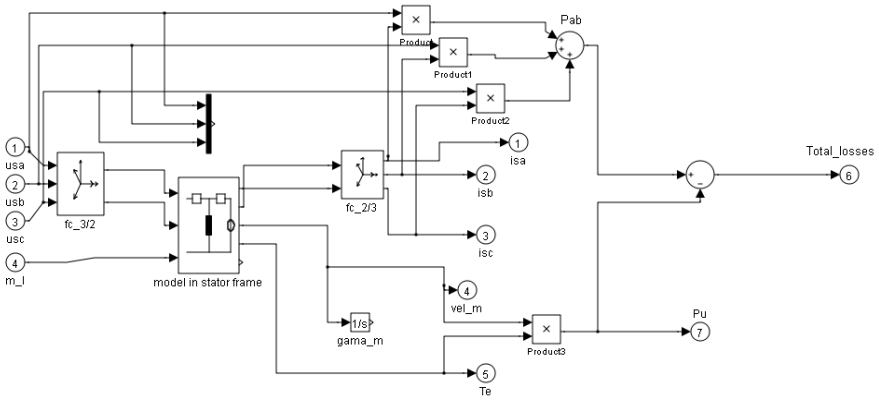

Figure 14. Induction motor model of figure 15 (stator d-q reference frame)

represents the load torque demanded by the drive cycle, while in the third one the motor limits and working points imposed by the drive cycle are illustrated, together with the most significant LMA´s efficiency gain zones. Finally, a table with LMA and conventional flux regulation energy performances is also presented.

From a general perspective, these results confirm the main LMA features, described in section 3.2 visible differences from conventional flux regulation occur for low load torque, particularly for relative low speeds. This agrees to the fact that in regions where I_{ds} has a large regulation flexibility, LMA and conventional flux regulation have clearly different performances.

5.1. ECE-R15

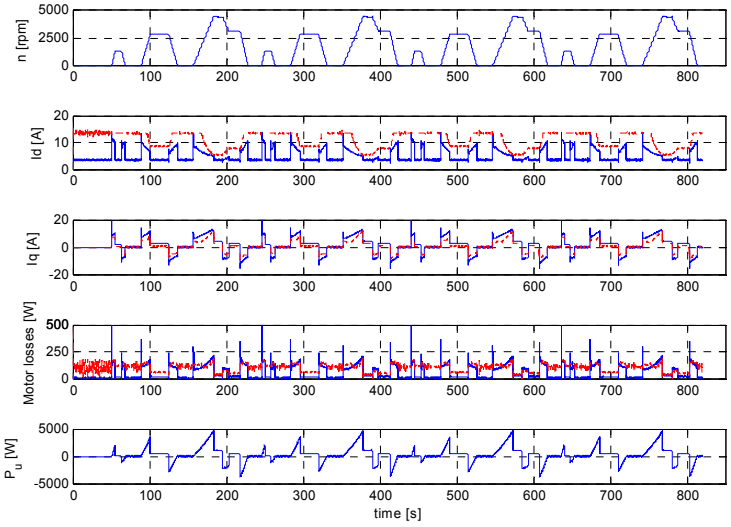

Figure 15. Drive-cycle; (I_d; I_q; Motor losses) – [blue:LMA; red dashed line: conventional regulation]; P_u

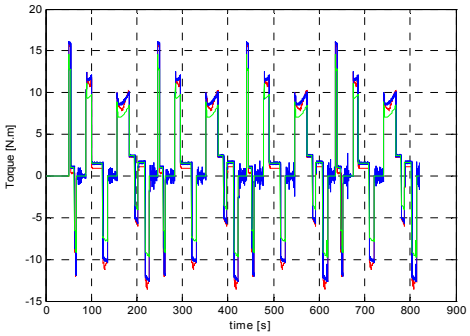

Figure 16. Torques [T_load (green); Te*(red); Te (blue)]

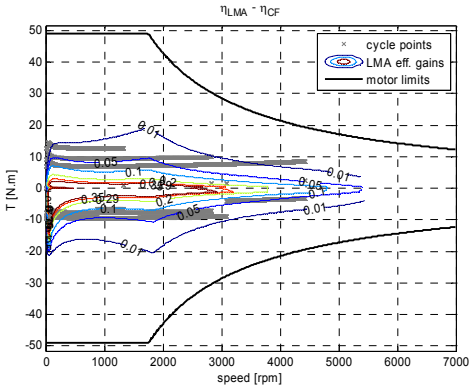

Figure 17. ECE-R15 drive cycle points over LMA efficiency curve gain

	Without LMA	With LMA
Eu (kJ)	221,8	221,5
Eab (kJ)	305,5	266,5
Motor losses (kJ)	83,7	45,0
Energy efficiency (%)	72,6	83,1

Table 5. ECE-R15 energy performances (Eu: energy supplied by the induction motor for the considered drive cycle; Eab: energy absorbed by the induction motor)

In almost 50% of the ECE-R15 drive cycle duration, motor speed is between 0 and 2000 rpm, with the motor torque among -13 Nm and 16 Nm (aprox.) – see figure 16. So, LMA inclusion allows significant loss reductions (table 5): with LMA, total losses are about 20% of E_u (energy supplied by the motor); without LMA, goes up to 38% of E_u. As expected, the main I_{ds} differences occur for n<2000 rpm, particularly for low torques (with LMA, smaller I_{ds} values are clearly visible). In a similar way, LMA performance in braking modes brings good results, since demanded torque has always low values. It should be pointed that when

the vehicle is immobilized (I_{qs}=0), LMA performance leads to very significant results (figure 15), since I_{ds} is regulated to its minimum value, while with conventional flux regulation, I_{ds} has its maximum value. In this case, motor iron losses are much higher when compared to the ones with LMA.

From an energy perspective, although LMA acts directly on the iron losses (since it regulates I_{ds}), it has also an impact in motor copper losses (as mentioned in section 3.2). Although for a given torque value, I_{qs} with LMA is higher than with conventional flux regulation (since I_{ds} is smaller), a better equilibrium between I_{ds} and I_{qs} is achieved with LMA. Since copper losses are also dependent on I_{ds}^2 and I_{qs}^2, the motor efficiency has a clear improvement in this drive cycle scenario, which may be seen from figure 17. Nevertheless, efficiency values are relative low, which is no surprise if one take into consideration the efficiency maps (figure 5) together with figure 17 (notice the efficiency (power) curve gains and cycle working points, particularly for n<2000 rpm).

5.2. Europe: City

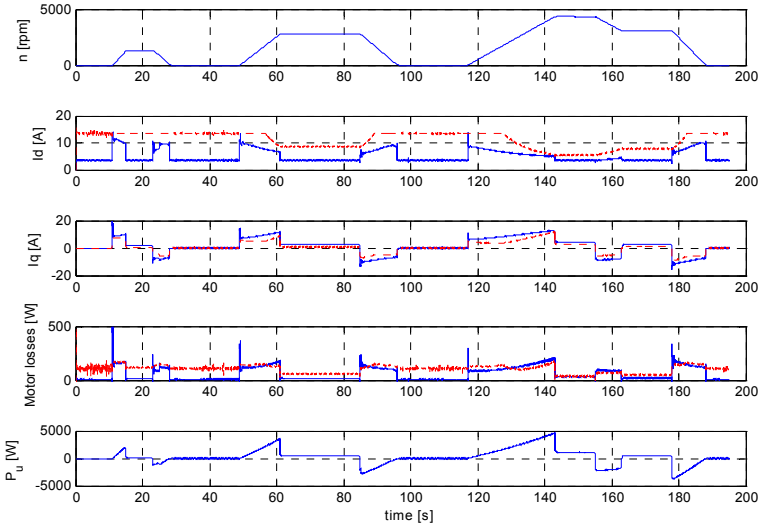

Figure 18. Drive-cycle; (Id; Iq; Motor losses) – [blue:LMA; red dashed line: conventional regulation]; P_u

For about 60% of total time of the "Europe: City" cycle, the vehicle speed is also below 2000 rpm, with the motor torque between -13 Nm and 16 Nm (aprox.). The vehicle is at rest for about 25% of the drive cycle duration. Basically, it puts the motor in the same (T,ω) working region as ECE-R15 (see figures 17 and 20). However, since it has a short time period (195 seg.), energy level demanded is much lower – the lowest one from the chosen drive cycle set. Similar relative energy losses are achieved: 20% for LMA and 36% without LMA of E_u (table 6). In both motor and braking modes, LMA most relevant results are in low speed – low torque region.

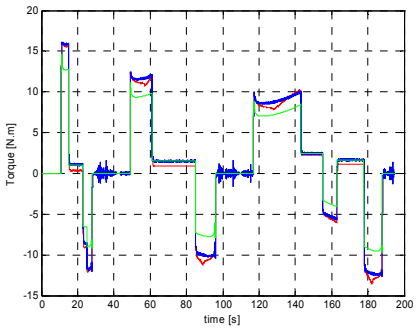

Figure 19. Torques [T_load (green); Te*(red); Te (blue)]

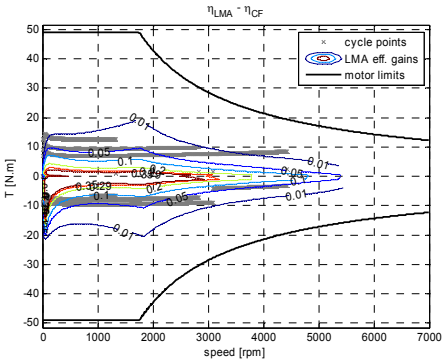

Figure 20. Europe: City drive cycle points over LMA efficiency curve gain

	Without LMA	With LMA
Eu (kJ)	55,5	55,4
Eab (kJ)	75,3	66,6
Motor losses (kJ)	19,8	11,2
Energy efficiency (%)	73,6	83,2

Table 6. Europe: City energy performances

The slightly efficiency increase for this cycle (when compared to ECE-R15) may be associated to the relative decrease of vehicle resting period (about 33% in ECE-R15).

5.3. 11 – Mode (Japan)

Drive cycle period where n<2000 rpm is relative short (<33%); the motor torque lies between 13 Nm and -10 Nm and the vehicle is immobilized a little less than 25% of the cycle duration. As expected, it´s in the initial resting time period and on the final 25 sec that I_{ds} values generated by the LMA are significantly different from the conventional flux I_{ds}

values. In other words, the motor losses difference are attached to these time periods, particularly to the resting one (figure 21). On the other drive cycle periods, motor losses are very similar (notice that in some intervals, LMA losses are slightly larger. This unexpected result is most probably related to the issue discussed in section 4.4).

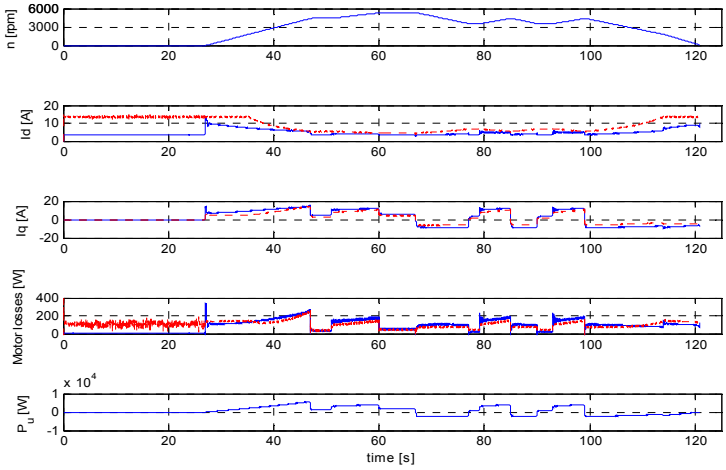

Figure 21. Drive-cycle; (Id; Iq; Motor losses) – [blue:LMA; red dashed line: conventional regulation]; P_u

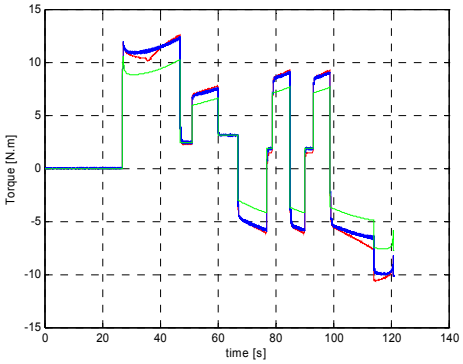

Figure 22. Torques [T_load (green); Te*(red); Te (blue)]

LMA total losses are about 14% of E_u, while conventional regulation losses are 16% of E_u. Although curve efficiency gains in figure 23 are referred to power efficiency, cycle working points somehow agree with efficiency energy gain achieved with LMA (table 7): for n> 2000 rpm there is a significant number of points between 1% and 5 % efficiency curves gain; also notice that some points are below 1% efficiency gain.

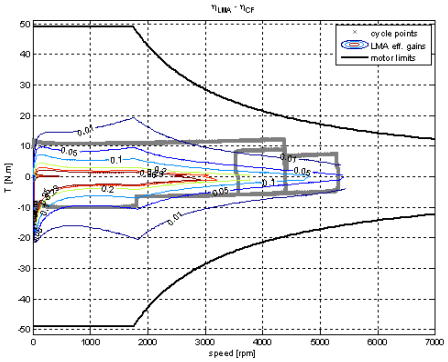

Figure 23. 11-Mode drive cycle points over LMA efficiency curve gain

	Without LMA	With LMA
Eu (kJ)	76,7	76,7
Eab (kJ)	89,3	87,5
Motor losses (kJ)	12,5	10,8
Energy efficiency (%)	86	87,6

Table 7. 11-Mode energy performances

5.4. FTP-75

For this drive cycle, the time period for which n<2000 rpm is shorter then the previous cycles. Motor torque limit is now -20 Nm and 25 Nm (aprox), while maximum speed is 8000 rpm. Frequent accelerations, as well as its long time period (1840 sec), make this cycle the most energy demanding. At the same time, pushes the motor to its limits: figure 24 shows that motor exceeds its nominal power between [200-300] s and later in the interval [1500-1700] sec. However, this overload (whose maximum instantaneous power is about 11 kW) occurs for a small number of intervals, each one with a very short existence. This way, it´s reasonable to assume that motor is not under electric hazardous working conditions. From a mechanical perspective, maximum speed - about 4 times motor nominal speed – is reached for relative short intervals, so one may assume that the motor (and the vehicle) will be safe in this working conditions.

Due to high speeds and relative high torque demand (figure 25), LMA shows a relative performance closer to the conventional regulation. As expected, relevant differences for I_d generation occur for relative low speed (basically, when the vehicle is at rest) and low torque values, e.g. intervals [50-200; 800-950] sec. – figures 25 and 26. With LMA and without it, motor losses are, respectively, 11,4% and 13,1% of E_u (table 8). Motor efficiency map (figure 5) explains the high efficiency values associated to this cycle, while the small efficiency gain achieved is according to figures 25 and 26.

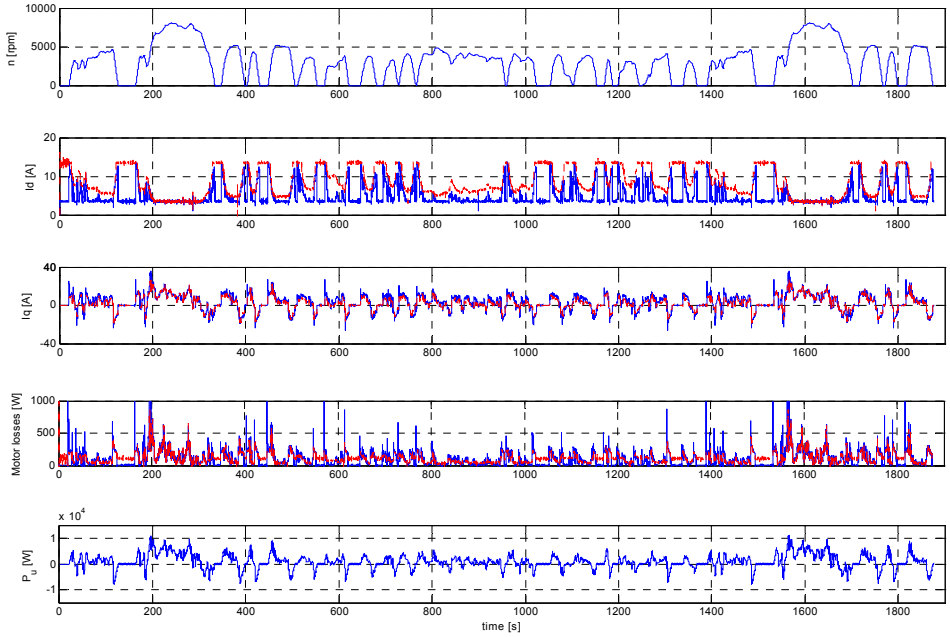

Figure 24. Drive-cycle; (Id*-red & Id-blue); (Iq*-red & Iq-blue); P_{ab} and motor losses (without LMA)

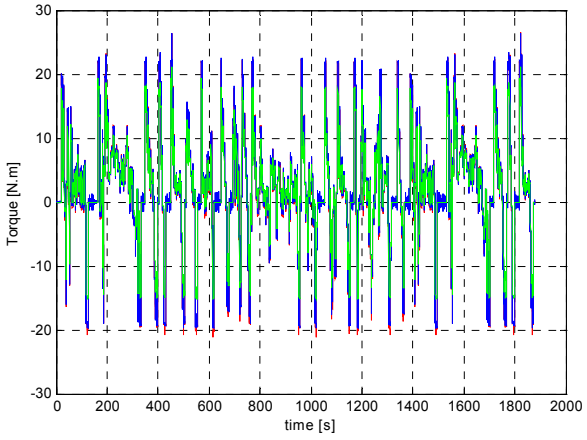

Figure 25. Torques [T_load (green); Te*(red); Te (blue)]

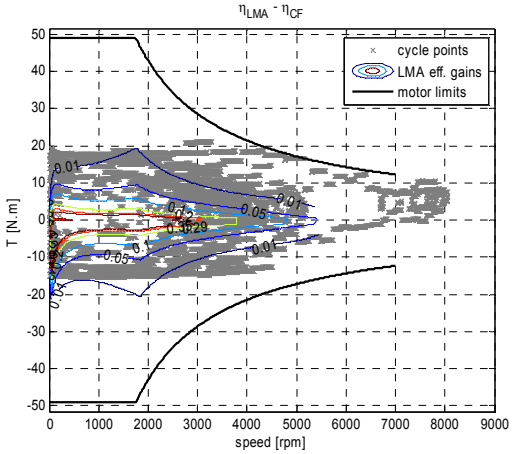

Figure 26. FTP-75 drive cycle points over LMA efficiency curve gain

	Without LMA	With LMA
Eu (kJ)	1716	1716
Eab (kJ)	1941	1910
Motor losses (kJ)	225,1	194,6
Energy efficiency (%)	88,4	89,8

Table 8. FTP-75 energy performances

Figures 27 and 28 present, respectively, induction motor energy consumption, efficiency and losses for each simulated drive cycle, with and without LMA.

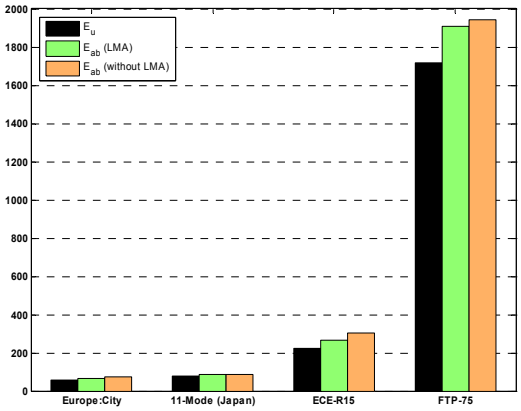

Figure 27. Drive-Cycles energy consumptions [kJ]

As a final remark, it is interesting to note that Europe:city and ECE-R15 have similar efficiency levels; also the same fact can be seen for 11-Mode and FTP-75.

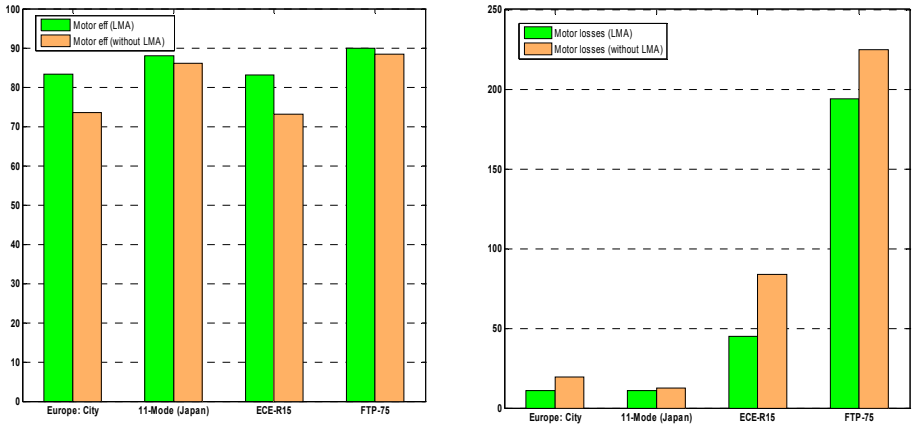

(a) (b)

Figure 28. Drive-Cycles energy efficiency [%] (a) and motor losses [kJ] (b)

6. Conclusion

Induction motor drives for EVs are submitted to a large set of working conditions, quite different from rated ones. Motor energy saving is fundamental for improving EVs performances. Under the loss model based approach previously discussed (LMA), a set of simulation results was presented in this book chapter, aiming to improve the induction motor energy performance. Different standard driving cycle scenarios were considered in order to evaluate the chosen LMA features: compared to conventional flux regulation, the major improvements in motor efficiency are for low load torque, particularly for relative low speeds. These are the motor working points where its efficiency is tipically lower, which is an interesting LMA feature. This is in agreement to the fact that LMA action has a more significative impact on ECE-R15 and Europe:city efficiencies, as explained through figures 15,17 and 18, 20 analysis.

Due to LMA impact on iron losses (function of I_d), a possibility to be considered in future works is the impact of LMA on motors with higher power rates and/or high efficiency level motors, where the relative weights of iron and copper losses are different.

Author details

Pedro Melo
Polytechnic Institute of Porto, Portugal

Ricardo de Castro and Rui Esteves Araújo
Faculty of Engineering – University of Porto, Portugal

7. References

Bazzi, A., & Krein, P. (2010). Review of Methods for Real-Time Loss Minimization in Induction Machines. *IEEE Transactions on Industrial Applications,* Vol.41, No.6, pp. 2319-2328.

Fernandez-Bernal, F., Garcia-Cerrada, A., & Faure, R. (2000). Model-based loss minimization for DC and AC vector-controlled motors including core saturation. *IEEE Transactions on Industrial Applications,* Vol.36, No.3, pp. 755-763.

Garcia, G., Luis, J., Stephan, R., & Watanabe, E. (1994). An efficient controller for an adjustable speed induction motor drive. *IEEE Transactions on Industrial Electronics*, Vol.41, No.5, pp. 533-539.

Guzzella, L., & Amstutz, A. (2005), *The QSS Toolbox Manual*, Measurement and Control Laboratory –Swiss Federal Institute of Technology Zurich.

Kioskeridis, I., & Margaris, N. (1996). Loss minimization in induction motor adjustable-speed drives. *IEEE Transactions on Industrial Electronics,* Vol.43, No.1, pp. 226-231.

Krishnan, R. (2001). *Electric Motor Drives – Modeling, Analysis and Control* (1 edition), Prentice Hall, ISBN 13: 978-0130910141.

Lim, S. and K. Nam (2004). Loss-minimising control scheme for induction motors. I*EE Proceedings - Electric Power Applications,* Vol.151, No.4, pp. 385-397.

Novotny, D., Lipo, T. (1996). *Vector control and dynamics of AC drives,* Clarendon Press, Oxford, ISBN 9780198564393.

Zeraoulia, M., M. E. H. Benbouzid, et al. (2006). Electric Motor Drive Selection Issues for HEV Propulsion Systems: A Comparative Study. *IEEE Transactions on Vehicular Technology*, Vol.55, No.6, pp. 1756-1764.